COBEM 2021 26th International Congress of Mechanical Engineering
November 22-26, 2021, Virtual Congress, Brazil
ABCM Associação Brasileira de Engenharia e Ciências Mecânicas

COB-2021-0882
PARAMETER IDENTIFICATION AND MODEL UPDATING OF THIN PLATE STRUCTURE WITH RECTANGULAR CUT BASED ON ITERATIVE METHODS AND OPTIMIZATION

Gabriel Godonhoto Kozikoski
Henrique Leandro Silveira
University of Lavras, Lavras, MG, Brazil
gabriel.kozikoski@estudante.ufla.br
henrique.silveira@ufla.br

Abstract. *To ensure an ideal engineering project it is necessary to realize different studies and tests in the structures, avoiding in many cases, noise, vibration and failure of aircraft, vehicles, industrial machines and equipment. Irregular plates are present in parts of these structures and it is often necessary to predict the dynamic behavior, understanding the system and possibly adjust them according to the application. Through a representation of the finite element method (FEM), it is possibly to construct a theoretical model of a plate with rectangular cut, identifying and adjusting the parameters of the model from a experimental model, as initially there is no good correlation due to imperfections in the geometry, material properties and boundary conditions. Furthermore, it is very important in this process to propose a damping model and identify its parameters, in such a way that represents the real behavior of the flexible structure. This paper presents and discusses the use of the Ewins-Gleeson method in the parameter identification of the model and makes a comparison between the particle-swarm-optimization (PSO) and differential evolution (DE) algorithms in the model updating process, discussing the main advantages of both formulations in the theoretical-experimental validation, with the experimental data being simulated from the FEM model.*

Keywords: *differential evolution, particle-swarm-optimization, iterative method, Ewins-Gleeson.*

1. INTRODUCTION

In engineering, several tools and studies were created through computational improvement and technology development. Vibration, noise and life cycle of equipment are extremely important, directly interfering with the cost and safety of structures, in view of this, analytical models that predict the experimental model are necessary, extracting important information from the components. Asymmetric thin plate structures have wide application in engineering, present in parts of aircraft, vehicles, industrial machines and various equipment.

Through the finite element method (FEM) it is possible to simulate the dynamics of asymmetric flexible structures. From that, a validation theoretical-experimental is necessary, validating with a model updating, adjusting the FEM model parameters. To the model updating this paper presents two iterative algorithms, differential evolution (DE) and particle-swarm-optmization (PSO), comparing their advantages, disadvantages and results.

Through the Ewins-Gleeson parameter identification technique it is possible to obtain modal parameters of undamped or lightly damped structures, assuming the hysteretic model, as a thin plate structure. This method is easy to implement, applicable to various structures and proven to be robust and reliable tool. Through the experimental structure it is possible to compare the theoretical model with the experimental one, checking the reliability (Ewins, 1982).

Iterative methods for updating models are easy to apply and efficient tools, being the most popular as they can be implemented in existing finite element codes (Chen and Ni, 2018). The differential evolution algorithm introduced by Storn and Price (1997), relies on mutation, recombination and selection to evolve the candidate solution collection, has been a good performance tool used in several engineering applications, being easily implemented in any computer language, requiring minimal parameter tuning (Das *et al.*, 2008).

Differential Evolution has been applied to many problems, demonstrating the tool's potential. Rogalsky *et al.* (2000) applied the method in aerodynamic shape optimization, obtaining the best fan blade design. Keshtkar *et al.* (2011) used it in optimization of rotor speed variations in microturbines. Doyle *et al.* (1999) applied in automated mirror design and Seyedpoor and Pahnabi (2021) evaluated the method for a beam and two planar frames.

In comparison, a alternative method is the particle swarm optimization (PSO), a common global optimization tool (Kennedy and Eberhart, 1995). PSO is a stochastic, population-based evolutionary algorithm based on socio-psychological principles, inspired in birds behavior, using group knowledge and individual knowledge. It has been very successful in

optimizing applied in many areas. Janson *et al.* (2008) implemented for molecular docking. Yisu *et al.* (2008) applied a PSO where a distribution vector was used in the update of the velocities of particles and Liu *et al.* (2007) used to a conceptual design.

All methods mentioned are robust, easy to implement and widely used in many areas. Many literature compared PSO and DE with other algorithms, demonstrating better results and advantages. Pradhan *et al.* (2021) compared PSO with others iterative algorithms, showing advantages and disadvantages of each technique. Le-Anh *et al.* (2015) presented static and frequency optimization of folded laminated composite plates comparing PSO, DE and genetic algorithm (GA) methods. Thus, the PSO and DE algorithms have shown excellent results.

2. THEORETICAL MODEL

A mechanical system can be modeled by its properties, such as mass, stiffness and damping, responsible for inertia, elastic and dissipative forces (Maia and Silva, 1997). A system with n degree of freedom can be expressed in canonical form by Eq. (1)

$$[M]\{\ddot{x}(t)\} + [D]\{\dot{x}(t)\} + [K]\{x(t)\} = \{f(t)\} \tag{1}$$

$$[D] = \varepsilon[K] + \tau[M] \tag{2}$$

where $[M]$ is the mass matrix, $[D]$ is the hysteretic damping matrix, Eq. (2), $[K]$ is the stiffness matrix and ε and τ are proportional constants. The $\{\ddot{x}(t)\}$, $\{\dot{x}(t)\}$ and $\{x(t)\}$ are are vectors of time-varying acceleration, velocity and displacement response respectively. The $\{f(t)\}$ is a time-varying vector representing external forces.

Assuming that the solution of Eq. (1) is the form expressed in Eq. (3)

$$\{x(t)\} = \{\bar{X}\}e^{i\lambda t} \tag{3}$$

where $\{\bar{X}\}$ is a vector of time-independent response amplitudes. Substituting Eq. (3) into Eq. (1), arrive at Eq. (4) for a free vibration solution.

$$[[K] - \lambda^2[M] + i[D]]\{\bar{X}\} = \{0\} \tag{4}$$

$$\lambda_r^2 = \omega_r^2(1 + i\,\eta_r) \tag{5}$$

Eq. (4) represents a complex eigenvalue problem, leading to eigenvalue, where λ^2 contains information of damping and natural frequencies squared, show in Eq. (5), and eigenvectors representing mode shapes.

2.1 Finite element method of thin plate

The mathematical model used is a thin plate structure based on the Kirchhoff-Love theory. This model has some assumptions that are analogous to the Euler-Bernoulli beam theory. The plate thickness is much smaller than its in plane dimensions and the deflection in perpendicular direction of the surface is much less than the thickness of the plate. Furthermore, the transverse shear strains are zero $\gamma_{xz} = \gamma_{yz} = 0$, normal strain, $\epsilon_z = 0$, normal stress σ_z has no effect on in-plane strains in the stress-strain equations, and in-plane forces are neglected (Logan, 2016).

Figure 1 presents the thin plate model schematic. Each node has three degree of freedom, one in a transverse displacement in z direction and two rotations about x and y axis, called w , θ_x and θ_y , respectively. So, each element has 12 degrees of freedom, three for each node, i , j , n and m. The rotations are related to the transverse displacement, as shown in Eq. (6).

$$\theta_x = +\frac{\partial w}{\partial y} \quad \theta_y = -\frac{\partial w}{\partial x} \tag{6}$$

The deflection w is considered a function of x and y , $w = w(x, y)$. The terms in the polynomial are selected according with the number of degree of freedom, represented in Eq. (7)

$$w = \alpha_1 + \alpha_2 x + \alpha_3 y + \alpha_4 x^2 + \alpha_5 xy + \alpha_6 y^2 + \alpha_7 x^3 + \alpha_8 x^2 y + \alpha_9 xy^2 + \alpha_{10} y^3 + \alpha_{11} x^3 y + \alpha_{12} xy^3 \tag{7}$$

The Eq. (8) represents the nodal coordinates as a function of the polynomial coefficients, general for each node.

$$\begin{Bmatrix} w \\ \theta_x \\ \theta_y \end{Bmatrix} = \begin{bmatrix} 1 & x & y & x^2 & xy & y^2 & x^3 & x^2y & xy^2 & y^3 & x^3y & xy^3 \\ 0 & 0 & +1 & 0 & +x & +2y & 0 & +x^2 & +2xy & +3y^2 & +x^3 & +3xy^2 \\ 0 & -1 & 0 & -2x & -y & 0 & -3x^2 & -2xy & -y^2 & 0 & -3x^2y & -y^3 \end{bmatrix} \begin{Bmatrix} \alpha_1 \\ \alpha_2 \\ \alpha_3 \\ \vdots \\ \alpha_{12} \end{Bmatrix}$$

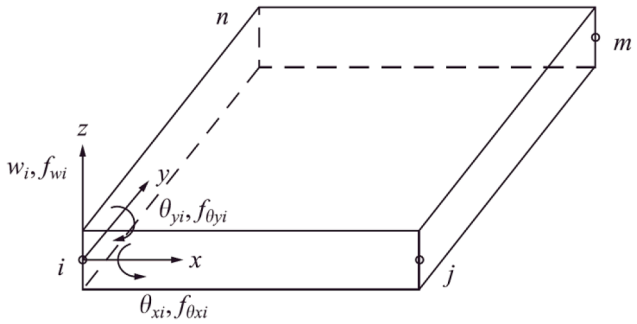

Figure 1. Basic rectangular plate element with nodal degrees of freedom. (Logan, 2016)

(8)

If Eq. (8) is evaluated for each node point, the general plate coordinates can be expressed as Eq. (9)

$$\{d\} = [C]\{\alpha\} \tag{9}$$

where $\{d\}$ is the 12 x 1 matrix, containing the degree of freedom of the plate and $[C]$ is the 12 x 12 matrix, containing all coordinates of each node.

Therefore, the constants can be found as Eq. (10), using the inverse of $[C]$ matrix.

$$\{\alpha\} = [C]^{-1}\{d\} \tag{10}$$

The Eq. (11) represents Eq. (8) in simple matrix form. Replacing the Eq. (10) into Eq. (11), results in Eq. (12).

$$\{\psi\} = [P]\{\alpha\} \tag{11}$$

$$\{\psi\} = [P][C]^{-1}\{d\} \tag{12}$$

$$[N] = [P][C]^{-1} \tag{13}$$

where $[N]$ is the shape function matrix, which correlates the displacement and slope of the element with the nodes.

Plate curvatures are established as the rate of change of angular displacements in relation to normals. They are expressed in Eq. (14) and Eq. (15) in matrix form.

$$\left\{ \begin{array}{c} \kappa_x \\ \kappa_y \\ \kappa_{xy} \end{array} \right\} = \left\{ \begin{array}{c} -\dfrac{\partial^2 w}{\partial x^2} \\ -\dfrac{\partial^2 w}{\partial y^2} \\ -\dfrac{2\partial^2 w}{\partial x \partial y} \end{array} \right\} = \left\{ \begin{array}{c} -2\alpha_4 - 6\alpha_7 x - 2\alpha_8 y - 6\alpha_{11} xy \\ -2\alpha_6 - 2\alpha_9 x - 6\alpha_1 0 y - 6\alpha_{12} xy \\ -2\alpha_5 - 4\alpha_8 x - 4\alpha_9 y - 6\alpha_{11} x^2 - 6\alpha_{12} y^2 \end{array} \right\} \tag{14}$$

$$\{\kappa\} = [Q]\{\alpha\} \tag{15}$$

Using Eq. (10) in Eq. (14), the curvature matrix can be expressed as

$$\{\kappa\} = [B]\{d\} \tag{16}$$

where

$$[B] = [Q][C]^{-1} \tag{17}$$

The usual form for a finite element stiffness matrix is given by Eq. (18)

$$[K] = \iint [B]^T [G][B] dx dy \tag{18}$$

where $[G]$ is the constitutive matrix given by Eq. (19) and $[B]$ is given by Eq. (17). E is Young modulus, ν is Poisson's coefficient and t is plate thickness (Bittencourt, 2010).

$$[G] = \frac{Et^3}{12(1-\nu^2)} \left[\begin{array}{ccc} 1 & \nu & 0 \\ \nu & 1 & 0 \\ 0 & 0 & \dfrac{1-\nu}{2} \end{array} \right] \tag{19}$$

For the mass matrix, the expression is given by Eq. (20), where ρ is the specific mass of the material and $[N]$ is given by Eq. (13).

$$[M] = \iint \rho [N]^T [N] dx dy \tag{20}$$

Then, the elementary mass matrix and stiffness matrix were demonstrated, being a function of physical properties. With these matrices it is possible to discretize the plate into finite elements.

2.2 Ewins-Gleeson parameter identification

The Ewins-Glesson Method is an indirect method of multiple degrees of freedom in the frequency domain, applied to structures lightly damped or with negligible damping, for a system of single input and single output (SISO) (Ewins, 1982). To determine the parameters that represent the experimental polynomial, such as natural frequencies, damping and eigenvector matrix, therefore, this method is considered simple and easy to implement (Maia and Silva, 1997).

The response at the j coordinate due to a single harmonic force excitation applied at the k coordinate, for a hysteretic model, can be expressed in accelerance terms, Eq. (21)

$$I_{jk}(\omega) = \frac{X_j}{F_k} = \sum_{r=1}^{\mathrm{N}} -\omega^2 \frac{\phi_{jr}\ \phi_{kr}}{\lambda_r^2 - \omega^2} \tag{21}$$

where the ϕ_{jr} and ϕ_{jr} are the mass-normalized mode shape vectors for each mode r, obtained from the eigenvector of Eq. (4) , λ^2 is the eigenvalue shown in Eq. (5), and ω^2 is the excitation frequency squared.

The accelerance $I_{jk}(\omega)$ can be rewritten as

$$I_{jk}(\omega) = \sum_{r=1}^{\mathrm{N}} \frac{\phi_{jr}\ \phi_{kr}}{1 - (\omega_r/\omega)^2(1 + i\ \eta_r)} \tag{22}$$

The Eq. (23) is the modal constant, represented by the numerator of Eq. (21).

$${}_rA_{jk} = \phi_{jr}\ \phi_{kr} \tag{23}$$

To calculate the N unknowns ${}_rA_{jk}$, it is necessary to select N discrete response frequencies $\Omega_1, \Omega_2, \ldots, \Omega_N$, different from natural frequencies, and organize them in a matrix assembly, Eq. (24). For this example, damping is negligible.

$$\begin{Bmatrix} I_{jk}(\Omega_1) \\ I_{jk}(\Omega_2) \\ \vdots \\ I_{jk}(\Omega_N) \end{Bmatrix} = \begin{bmatrix} \frac{1}{1-\omega_1^2/\Omega_1^2} & \frac{1}{1-\omega_2^2/\Omega_1^2} & \cdots & \frac{1}{1-\omega_N^2/\Omega_1^2} \\ \frac{1}{1-\omega_1^2/\Omega_2^2} & \frac{1}{1-\omega_2^2/\Omega_2^2} & \cdots & \frac{1}{1-\omega_N^2/\Omega_2^2} \\ \vdots & \vdots & \ddots & \vdots \\ \frac{1}{\omega_1^2-\Omega_N^2} & \frac{1}{\omega_2^2-\Omega_N^2} & \cdots & \frac{1}{\omega_N^2-\Omega_N^2} \end{bmatrix} \begin{Bmatrix} {}_1A_{jk} \\ {}_2A_{jk} \\ \vdots \\ {}_NA_{jk} \end{Bmatrix} \tag{24}$$

Eq. (24) can be rewritten in short form

$$\{I_{jk}(\Omega)\} = [R]\{A_{jk}\} \tag{25}$$

The matrix $[R]$ contains terms of natural frequencies and selected response frequencies. By inverting this matrix it is possible to identify modal constants as shown in Eq. (26)

$$\{A_{jk}\} = [R]^{-1}\{I_{jk}(\Omega)\} \tag{26}$$

Through the modal constants it is possible to extract the components of the modal matrix and thus reconstruct the complete experimental model, represented by the modal and spectral matrix.

2.3 Differential evolution (DE)

Storn and Price (1997) proposed a global optimization algorithm, belongs to the class of evolutionary algorithms (EAs), based on mutation, recombination and selection of candidate solutions, the differential evolution (DE). Starting with a population, like any evolutionary algorithm, which are initial solutions to the problem, set based on boundary

conditions previously chosen, that would be replaced with more improved generations. The Eq. (27) shows a random generator.

$$x_{i,j}(G) = x_j^L + rand(0,1)(x_j^U - x_j^L) \tag{27}$$

where $rand(0,1)$ is a random number lying between 0 and 1, x_j^L is a lower bound and x_j^U is an upper bound of the variable.

Now, DE performs some changes and combinations of variable vectors. To create a mutation, three parameter vectors are randomly chosen. For this, a scalar number F scales the difference between two of three vectors, adding to the third one. The mutation vector is expressed in Eq. (28)

$$v_{i,j}(G+1) = x_{3,j} + F(x_{1,j} - x_{2,j}) \tag{28}$$

In the binomial crossover, the vector is arranged with a mutant vector and a random number between 0 and 1 is compared with the CR value and evaluated in conditional form, as shown in Eq. (29). A crossover probability $CR \in [0,1]$ is selected by the user.

$$u_{i,j}(G+1) = \begin{cases} v_{i,j}(G+1);\ rand(0,1) \leqslant CR \\ x_{i,j}(G) \end{cases} \tag{29}$$

The next step is to select which of the target vectors will survive the next generation. This selection process is demonstrated in Eq. (30)

$$x_{i,j}(G+1) = \begin{cases} u_{i,j}(G);\ f(u_{i,j}) \leqslant f(x_{i,j}) \\ x_{i,j}(G) \end{cases} \tag{30}$$

where $f(u_{i,j})$ or $f(x_{i,j})$ is the function to be minimized, represented by the error function of the FRFs. By selecting a better value from the objective function, it replaces, improving the solution or remaining constant.

2.4 Particle-swarm-optimization (PSO)

Developed by Kennedy and Eberhart (1995), this algorithm starts with a population of random candidates, called particle. Each particle has a random velocity and position associated, and at each step the fitness function is evaluated . The best position is called $pbest_i$ and the best particle in the swarm is called $gbest(k)$. The Eq. (31) is the subsequent velocity of a particle i.

$$v_i(k+1) = \gamma\nu_i(k) + c_1 r_1(pbest_i - p_i(k)) + c_2 r_2(gbest(k) - p_i(k)) \tag{31}$$

where γ is the inertia of the particle, c_1 and c_2 are the "trust" parameters, previously chosen by the user, and r_1 and r_2 are random numbers between 0 and 1. The Eq. (32) is the subsequent position of a particle i.

$$p_i(k+1) = p_i(k) + \nu_i(k+1) \tag{32}$$

After calculating the position and velocity, the algorithm repeats these processes until convergence.

The PSO algorithm has wide application and some advantages such as: it is easy to execute, it can be easily implemented using parallel processing, it does not require the calculation of the objective function derivatives, it contains a small number of adjustable parameters and it is an effective algorithm for identifying a global optimum solution (Marwala, 2010).

3. COMPUTER SIMULATION

3.1 Model updating

A simulated numerical model is used to represent the experimental model, performing as a physical structure. For a real thin plate, an elastic nylon wire is used to suspend the plate, simulating the free-free condition in a typical modal test. The structure has four contact points, so a nylon stiffness and nylon damping are added to a stiffness and damping matrix, respectively, also a mass accelerometer and the FRF numeric signal was contaminated with white noise to simulate the effect of any noise present in an experimental measurement.

The Eq.(33) shows the objective function that represents the difference between theoretical and experimental FRFs used to update the model for both algorithms.

$$S_{of} = \sum_{n=1}^{\mathrm{N}} \left(\frac{\left\| FRF_n^{exp} - FRF_n^{theo} \right\|}{\left\| FRF_n^{exp} \right\|} \right) \tag{33}$$

where S_{of} is the objective function value, FRF_n^{exp} is the simulated experimental function and FRF_n^{theo} is the analytical function of the FE model.

The Figure (2a) is the representation of the finite element plate with rectangular cut, discretized by 92 elements and 113 nodes. The plate geometry is (in SI units): a square plate with $0.48\mathrm{m}$, thickness of $0.0027\mathrm{m}$ and rectangular cut $(0.192\mathrm{x}0.096)\mathrm{m}$, represented by the steel $SAE1020$. The Figure (2b) shows the driving point FRF simulated. A hysteretic damping is used to represent the structure, assuming that damping is proportional to a stiffness matrix, Eq. (2), where $\tau = 0$.

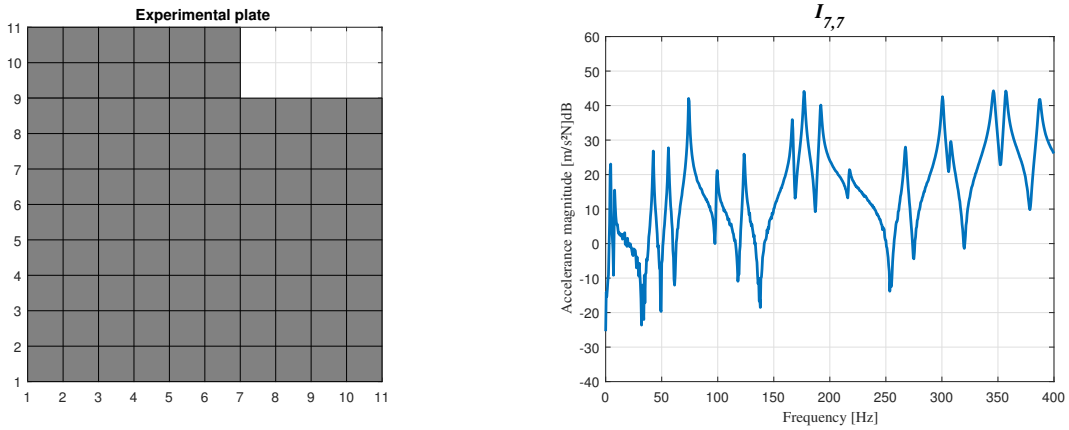

Figure 2. a) Experimental plate representation; b) Experimental simulated FRF.

Both algorithm have the same number of 50 iterations and 30 individuals for the initial population. For DE parameters, the crossover probability $CR = 0.2$ and for PSO the inertia of the particle $\lambda = 0.99$ and the acceleration coefficients $c_1 = c_2 = 0.2$.

The Figure (3) presents the updated FRF using the differential evolution algorithm and the Figure (4) presents the FRF using the particle-swarm optimization algorithm. Regardless of excitation point (k), both algorithms represented the experimental simulated FRF, however, for the FRFs with the PSO algorithm, the amplitudes at low frequencies had a slight discrepancy when compared to the FRFs of DE algorithm, justified by the nylon damping difference.

The Table (1) shows the parameters updated with their respective ranges. Mass, plate geometry and density are known, since they can be easily measured and calculated. The Young's modulus, nylon stiffness, nylon damping and the proportional coefficient are more difficult parameters to be found, justifying their use in the model updating.

Both algorithm were efficient, had a good convergence in the model updating and low computational cost. DE had values close to those simulated for Young's modulus, nylon stiffness and nylon damping, with relative errors smaller than PSO. Both are easy to execute and contain a small number of adjustable parameters, but DE algorithm is more robust, requires less computational cost and has a faster convergence. The Table (2) shows the comparison of parameters with the respective relative errors between the updated parameter and the simulated one.

Table 1. Model Updating parameters.

Parameters	Properties	Limits	
Young Modulus	$\mathrm{E(N/m^2)}$	150E+09	250E+09
Nylon stiffness	Kn (N/m)	100	2000
Nylon damping	Cn (Ns/m)	1E-04	1.5
Hysteretic coefficient	ε	1E-06	1E-02

Table 2. Parameters comparison between experimental, DE, PSO and respective relative errors.

Parameters	Parameters simulated	DE	DE error	PSO	PSO error
Young Modulus $\mathrm{E(N/m^2)}$	200.00E+09	199.49E+09	2.55E-03	199.48E+09	2.60E-03
Nylon stiffness (N/m)	900.00	903.67	4.08E-03	889.56	1.16E-02
Nylon damping (Ns/m)	1.00	1.09	9.00E-02	0.80	2.00E-01
Hysteretic coefficient	5.00E-03	6.10E-03	2.20E-01	6.10E-03	2.20E-01

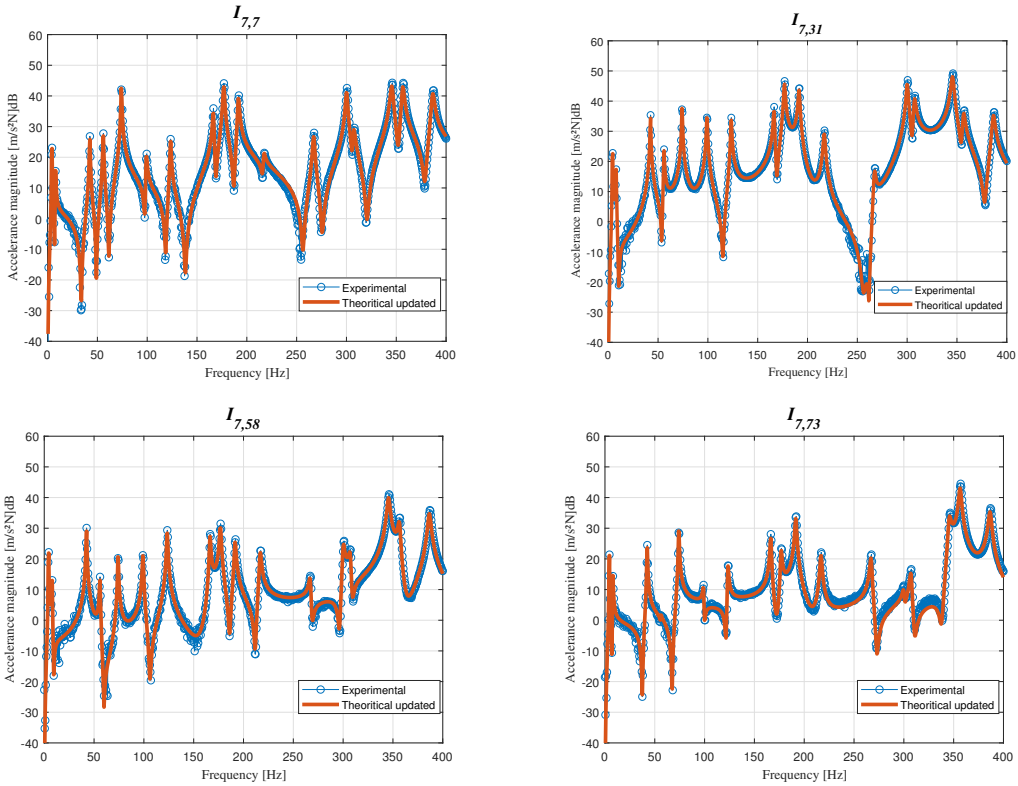

Figure 3. Analitical FRF updated using differential evolution.

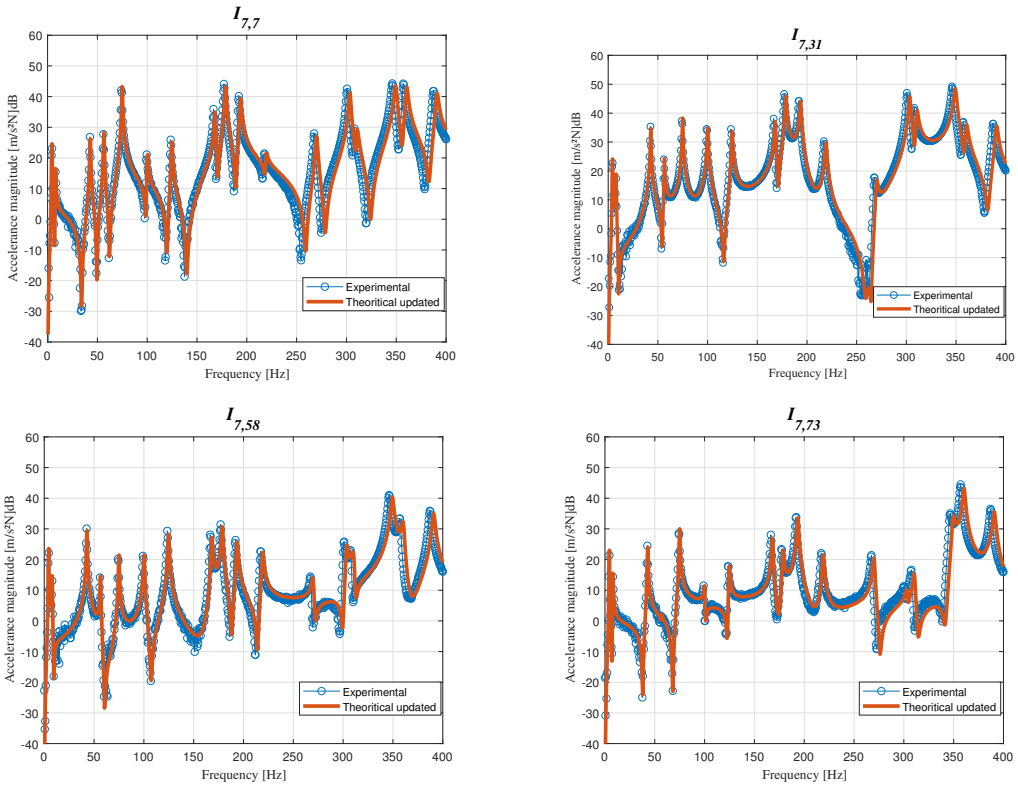

Figure 4. Analitical FRF updated using particle-swarm-optimization.

3.2 Parameter identification from Ewins-Gleeson method

The selected data for the frequencies should not equal the anti-resonance and resonance. The chosen sampled points (Ω) are the natural frequencies added a $\delta\Omega$. The accelerance amplitudes $I_{jk}(\Omega)$ are chosen based on the points sampled.

Assembling the matrix $[R]$ demonstrated in Eq. (24), it is possible obtain the modal constants as Eq. (26). The response curve can be regenerated from the experimental modal constants found, this regenerated curve should correspond to the original response curve, demonstrating an efficient method. The regenerated FRF accurately describes the experimental simulated FRF qualitatively, shown in Figure (5).

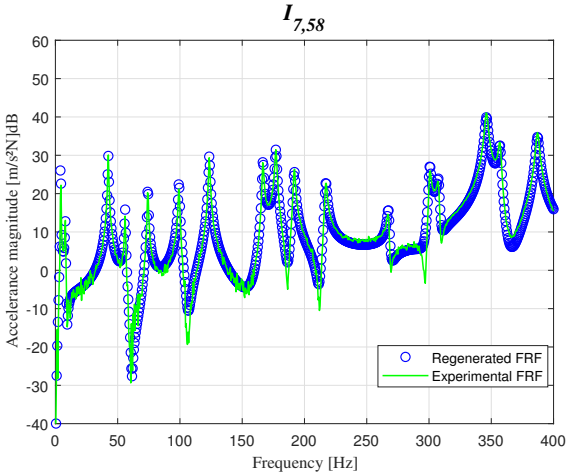

Figure 5. Regenerated and experimental FRF.

The modal matrix can be reconstructed from the modal constants, using the square root of the modal constant at the driving point, thus, easily calculating the other terms of the modal matrix.

The Fig. (6) compared the regenerated FRF with the PSO, DE and experimental simulated FRFs. The Ewins-Gleeson method curve closely approximates to the others, with a slightly difference in anti-resonance at approximately 250 Hz, probably because the frequency points sampled in this area are not the best.

Through the Ewins-Gleeson method it is possible to obtain the modal model without needing prior knowledge of the FEM model, different from the iterative methods.

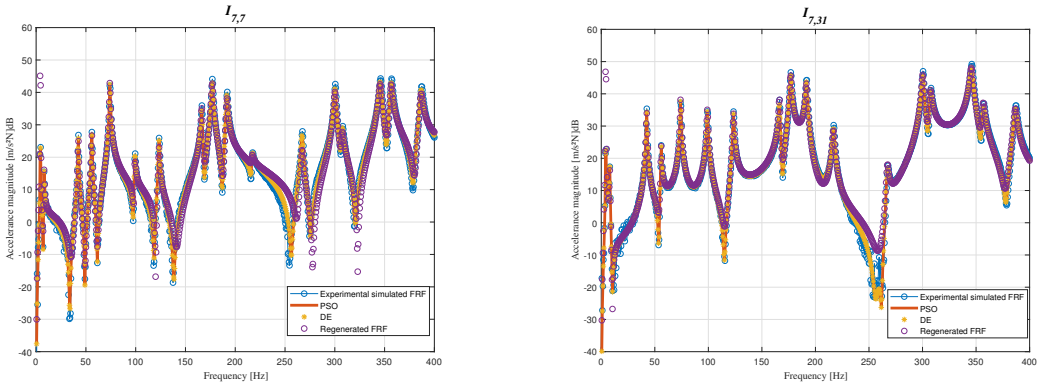

Figure 6. Experimental simulated, PSO, DE and regenerated FRFs.

4. CONCLUSION

By investigating the numerical results, the updated theoretical model accurately represented the simulated experimental model. Even for a low population size and iterations, comparing Figure (3) and Figure (4), the two algorithms converged for the parameters simulated. For better results it would be necessary a higher number of iterations, but the model updating was satisfactory even though DE converged faster, solving structural optimization problems.

The Ewins-Gleeson method achieved good results, even comparing qualitatively between regenerated and experimental FRF and with PSO and DE model updated. It was observed that this method is extremely sensitive to the sampled frequency points, but it is easy and simple to calculate the modal parameters.

5. REFERENCES

Allemang, R., Rost, R. and Brown, D., 1982. "Dual input estimation of frequency response functions for automotive structures". Technical report, SAE Technical Paper.

Avitabile, P., 2017. *Modal testing: a practitioner's guide*. John Wiley & Sons.

Bittencourt, M., 2010. "Analise computacional de estruturas: Com aplicaÇao do metodo de elementos finitos". *IEEE Transactions on Magnetics*, Vol. 36, No. 4, p. 1009– 1013.

Chen, H.P. and Ni, Y.Q., 2018. *Structural health monitoring of large civil engineering structures*. Wiley Online Library.

Das, S., Abraham, A. and Konar, A., 2008. "Particle swarm optimization and differential evolution algorithms: technical analysis, applications and hybridization perspectives". In *Advances of computational intelligence in industrial systems*, Springer, pp. 1–38.

Doyle, S., Corcoran, D.A. and Connell, J., 1999. "Automated mirror design using an evolution strategy". *Optical Engineering*, Vol. 38, No. 2, pp. 323–333.

Ewins, D.J., 2000. *Modal testing: theory, practice and application*. Research Studies Press.

Ewins, D. J.; Gleeson, P.T., 1982. "Method for modal identification of lightly damped strucutures". *Journal of Sound and Vibration*, Vol. 84, No. 1, pp. 57–79.

Friswell, M. and Mottershead, J.E., 2013. *Finite element model updating in structural dynamics*, Vol. 38. Springer Science & Business Media.

Fu, Z.F. and He, J., 2001. *Modal analysis*. Elsevier.

Janson, S., Merkle, D. and Middendorf, M., 2008. "Molecular docking with multi-objective particle swarm optimization". *Applied Soft Computing*, Vol. 8, No. 1, pp. 666–675.

Kennedy, J. and Eberhart, R., 1995. "Particle swarm optimization". In *Proceedings of ICNN'95-international conference on neural networks*. IEEE, Vol. 4, pp. 1942–1948.

Keshtkar, H., Alimardani, A. and Abdi, B., 2011. "Optimization of rotor speed variations in microturbines". *Energy Procedia*, Vol. 12, pp. 789–798.

Le-Anh, L., Nguyen-Thoi, T., Ho-Huu, V., Dang-Trung, H. and Bui-Xuan, T., 2015. "Static and frequency optimization of folded laminated composite plates using an adjusted differential evolution algorithm and a smoothed triangular plate element". *Composite Structures*, Vol. 127, pp. 382–394.

Liu, X., Liu, H. and Duan, H., 2007. "Particle swarm optimization based on dynamic niche technology with applications to conceptual design". *Advances in Engineering Software*, Vol. 38, No. 10, pp. 668–676.

Logan, D.L., 2016. *A first course in the finite element method*. Cengage Learning.

Maia, N. and Silva, J., 1997. *Theoretical and Experimental Modal Analysis*. Research Studies Press,.

Marwala, T., 2010. *Finite element model updating using computational intelligence techniques: applications to structural dynamics*. Springer Science & Business Media.

Pradhan, A., Bisoy, S.K. and Das, A., 2021. "A survey on pso based meta-heuristic scheduling mechanism in cloud computing environment". *Journal of King Saud University-Computer and Information Sciences*.

Rogalsky, T., Kocabiyik, S. and Derksen, R., 2000. "Differential evolution in aerodynamic optimization". *Canadian Aeronautics and Space Journal*, Vol. 46, No. 4, pp. 183–190.

Seyedpoor, S. and Pahnabi, N., 2021. "Structural damage identification using frequency domain responses and a differential evolution algorithm". *Iranian Journal of Science and Technology, Transactions of Civil Engineering*, Vol. 45, No. 2, pp. 1253–1264.

Storn, R. and Price, K., 1997. "Differential evolution–a simple and efficient heuristic for global optimization over continuous spaces". *Journal of global optimization*, Vol. 11, No. 4, pp. 341–359.

Yisu, J., Knowles, J., Hongmei, L., Yizeng, L. and Kell, D.B., 2008. "The landscape adaptive particle swarm optimizer". *Applied Soft Computing*, Vol. 8, No. 1, pp. 295–304.

6. RESPONSIBILITY NOTICE

The authors are solely responsible for the printed material included in this paper.